DOI:10.31557/APJCB.2026.11.2.547

RESEARCH ARTICLE

A Single-Cell Immune Topography Identifies CAF-Driven Checkpoint Inhibitor Failure in EGFR-TKI-Resistant Lung Cancer

Semaa A. Shaban[1], Mohammed Abd Hassan[1], Ban Hamid Khalaf[2], Ahmed AbdulJabbar Suleiman[3]

[1]Biology department, College of Science, Tikrit University, Tikrit, Iraq. [2]College of Pharmacy, University of Anbar, Anbar, Iraq. [3]Biotechnology Department, College of Science, University of Anbar, Anbar, Iraq.

Abstract

Background: The heterogeneity of responses to immune checkpoint inhibitors in non-small-cell lung cancer (NSCLC) after failure of EGFR-TKIs (tyrosine kinase inhibitors) is poorly understood as it relates to the tumor microenvironment (TME) and/or cancer-associated fibroblasts (CAFs) contributing to resistance against ABCP therapy. **Methods:** To investigate these questions, we analyzed seven patients who have failed EGFR-TKI therapy using pretreatment pleural effusions: three who responded, and four who did not. Pre-treatment effusions were processed via single-cell RNA sequencing (GSE233203). Data were processed using Seurat v5 and annotated using scType. Analyses performed included cell proportion modelling, immune module scoring, sub-clustering of CAFs, differential gene expression analysis, and pathway enrichment. **Results:** A total of 23 cellular clusters were identified from the seven patients. Non-responders exhibited a stromal-dominant and immune-excluded TME featured by high numbers of fibroblasts and mesothelial cells; while responders exhibited an immune-inflamed TME featured by cytotoxic T-cell activity. CAF analysis identified nine distinct CAF sub-types, with non-responders having the highest abundance of vCAF and ECM+ CAF and GREM1+ CAF populations. Non-responder CAFs exhibited the upregulation of 1,311 genes, of which a subset was previously characterized as associated with ECM remodeling (extracellular matrix), cytoskeletal organization, and/or neurogenic-like pathways (NRP2, BDNF, and DKK1). **Conclusion:** Our results suggest that the TME composition prior to initiating ABCP therapy is predictive of response to therapy. Further, our results suggest that programs driven by CAFs, such as stromal programs that promote immune exclusion and resistance, may hinder the efficacy of immunotherapy and therefore targeting the heterogeneity of CAFs may improve patient outcomes.

Keywords: NSCLC- Cancer-Associated Fibroblasts (CAFs)- Tumor Microenvironment (TME)- Therapy Resistance

Asian Pac J Cancer Biol, **11 (2)**, 547-557

Submission Date: 02/22/2026 Acceptance Date: 04/06/2026

Introduction

The global burden of cancer continues to escalate, posing a profound public health challenge. For the year 2022, it has been estimated a number of approximately 19.9 million new cancer cases and 9.7 million cancer-related deaths occurred worldwide [1].

The International Agency for Research on Cancer has stated that the number of new cancer diagnoses each year is expected to increase. By 2050, there may be over 35 million new cases of cancer annually, which is primarily due to the fact that lung cancer remains the most prevalent cancer (12.4%), and breast cancer and colorectal cancer follow (11.6% and 9.6%, respectively). However, recent trends are indicating that the way we identify and treat cancer is rapidly changing, and there is a need for improved and more effective treatments and therapies [2].

In recent years, immune checkpoint inhibitors (ICIs) have changed the way we treat cancer and have produced durable responses across a broad range of cancer types. On the other hand, another significant issue facing cancer patients today is that many will not respond to treatment

Corresponding Author:
Dr. Ahmed AbdulJabbar Suleiman
Cancer Biotechnology Department, College of Science, University of Anbar, Anbar, Iraq
Email: ahmed.suleiman@uoanbar.edu.iq

and/or will experience tumor relapse [3-5]. Additionally, the obstacles to effective treatment are not just related to the tumors [1-5] but rather include an examination of the complexity of the tumor microenvironment (TME) [6, 7].

In the TME, a variety of non-cancerous stromal cells produce an array of signals that promote tumour expansion. Among these, Cancer-Associated Fibroblasts (CAFs) are currently emerging as critical players in enhancing tumor progression, metastasis and therapy resistance. CAFs are today mainly considered as active craftsmen of the TME. Their greater abundance in stroma-rich and therapy-refractory tumors emphasizes their role as a cellular compartment [8-11]. This influence is exerted through the physical remodelling of tumour architecture, largely via excess deposition of collagen and by secretion of a wide array of chemical factors (including key cytokines and chemokines) that teach an immunosuppressive, pro-tumoral state by programming a pro-tumoral phenotype [12-14].

CAFs are of particular importance to immunotherapy, as they provide a stromal barrier that dampens ICIs by two main mechanisms. 19 First, CAFs constitute a physical barrier with the help of a tight extracellular matrix network (mainly collagen) that creates a physical blockade for CTL cells to attack the tumor. Second, inflammatory CAFs secrete a 'chemical fence' of immunosuppressive signals (TGF-β, IL-6 and CXCL12) that recruit regulatory T-cells (Tregs), trap T-cells in the stroma, as well as directly promoting exhaustion, which make immune cells irresponsive to therapy [15-17].

Importantly, these CAF-seeking functions are not solely confined to immune resistance. Work in EGFR-mutant NSCLC has demonstrated a causal relationship between the emergence of TKI resistance. Consequently, investigations into the components that make up the TME are now becoming central to solving such basic problems in oncology [18-20]. There is however large void in our understanding of which exact cellular and molecular 'determinants' are established prior to treatment commencement that will then determine a patient's subsequent response or resistance to real-world complex combinations. Although the presence of different immune-reactive immune-inflamed (sensitive) and immune-excluded (resistant) TMEs is known [21], the specific repertoire gene expression of CAF subsets that define these phenotypes have not been well-defined in a multiple drug therapeutic regimen.

The rationale for this study is to leverage high-resolution single-cell data to bridge this gap. We aim to deeply characterize the pre-treatment TME by dissecting these fundamental differences, we seek to uncover gene expression profiles and biomarkers of the non-response-associated CAF compartments compared to response-associated CAFs potential therapeutic targets to overcome this CAF-mediated resistance. To investigate this, our study will perform a detailed analysis of publicly available single-cell transcriptomic data from a clinically relevant cohort of patients with EGFR-TKI-resistant Non-small cell lung cancer (NSCLC), taken before they received ABCP (atezolizumab, bevacizumab, carboplatin, and paclitaxel) therapy. Therefore, this study provides a detailed, high-resolution view of the cellular and molecular features that define these two opposing TME states before the first dose of therapy.

Materials and Methods

Single-Cell Dataset Collection and Preprocessing

Single-cell transcriptome analysis was performed on pleural effusion samples acquired from seven patients with EGFR-TKI-resistant non-small cell lung cancer prior to the initiation of ABCP (atezolizumab, bevacizumab, carboplatin, and paclitaxel) therapy. Following treatment, patient outcomes were observed, and the pre-treatment samples were retrospectively grouped based on therapeutic response (3 responders, 4 non-responders), by the original authors of the study (Hong et al.). Count data for these samples were downloaded from the Gene Expression Omnibus (GEO: GSE233203) including the associated clinical metadata. Individual Seurat objects (Seurat v5) were created for each sample using ReadMtx and CreateSeuratObject with minimum cell and feature cutoffs (min.cells = 3, min.features = 200) [22]. Clinical and sample metadata, including GSM ID and therapeutic Response, were integrated into the meta.data slot of each object, and all individual objects were subsequently merged into a single, cohort-wide Seurat object for analysis. The percentage of mitochondrial gene expression (percent.mt) was calculated for each cell. Low-quality cells and potential doublets were filtered and removed from the merged object based on the following stringent criteria: nFeature_RNA > 200, nFeature_RNA < 6000, nCount_RNA > 1000, and percent.mt < 10.

Data Normalization, Dimensionality Reduction, and Clustering

The filtered cohort data was normalized using the NormalizeData function with a "LogNormalize" method and a scale factor of 10,000. The top 2,000 most highly variable genes (HVGs) were identified using FindVariableFeatures ("vst" method). The data was then scaled and centered using ScaleData. Principal Component Analysis (PCA) was performed on the HVGs, utilizing the top 50 principal components (PCs) for subsequent dimensionality reduction and clustering. A Uniform Manifold Approximation and Projection (UMAP) was generated for visualization. Cell clusters were identified using FindNeighbors (based on the top 50 PCs) and FindClusters (resolution = 0.9).

Initial Cohort-Wide Cell Type Annotation

The The scType marker-based approach [23] provided the initial annotation of cell types in all cells. The scType computational approach calculates a "scType score" for each cell type in relation to their respective clusters. It begins with a query from a tissue specific marker database ("Lung") containing both positive and negative marker genes. After the database is queried, the scType approach calculates a marker enrichment score for each cell by summing the z-score transformed expression values

of positive markers and subtracting this from the sum of the z-score transformed expression values of negative markers. The marker enrichment score will be defined by the positive and negative marker genes in the tissue specific marker database and be used to compute a global scType scores for each cell type. The cluster will take the cell type identity of the highest scType score.

Cohort-Wide Compositional Analysis

Using all types of cells to proportionately assess the total cellular makeup of the tumour microenvironment (TM) and comparing the make-up of the "Responders" vs. "Non-Responders" allowed for both types of analysis. The analysis for the comparison of the two groups was completed using General Linear Models (GLMs). GLMs were fitted with a quasibinomial family using raw cell counts per sample for each cell type using a glm model defined as cbind (cell type count, other cell type count) ~ Response provides an appropriate way to model proportion data and accounts for overdispersion in the response variable. False Discovery Rate (FDR) correction was used to adjust for multiple comparisons, and a faceted boxplot was used to display corrected p-values.

Preliminary Immune Function Analysis

To initially assess the functional status of the overall immune compartment and characterize the observed difference in TME type (hot vs. cold), module scores were calculated using the AddModuleScore function on cells globally annotated as "Immune system cells." Four key T-cell and myeloid signatures were tested: CD8+ Cytotoxicity (CD3D, CD3E, CD8A, CD8B, GZMA, GZMB, PRF1), T-cell Exhaustion (PDCD1, CTLA4, LAG3, TIGIT, HAVCR2), Regulatory T-cell (Treg) (CD4, FOXP3, IL2RA, CTLA4), and MDSC (S100A8, S100A9, CD33, IL4R, ARG1). Scores were visualized using violin plots and statistically compared between the "Response" and "Non-response" groups using the Wilcoxon rank-sum test.

Sub-clustering and Manual Annotation of the Fibroblast Compartment

A focused sub-clustering analysis was performed exclusively on cells initially annotated as "Fibroblasts." This subset was re-clustered, and cluster-defining markers were identified using the FindAllMarkers function. Based on the expression of these markers, eight distinct CAF subtypes were manually annotated. Proportional composition of these manually curated subtypes was visualized by condition using stacked bar charts.

Differential Gene Expression (DGE) Analysis of Fibroblasts

To identify transcriptional differences within the entire fibroblast compartment, DGE analysis was performed using the FindMarkers function implemented in Seurat v5. The contrast was specifically defined as "Non-response" versus "Response", grouping the cells by the Response metadata column. Genes significantly upregulated in the non-response group were identified based on the criteria: avg_log2FC > 0.25 and p_val_adj < 0.05.

Functional and Pathway Enrichment Analysis

The list of significantly upregulated genes from the non-responding fibroblasts was subjected to Over-Representation Analysis (ORA) to identify enriched biological functions and pathways. ORA was performed using the clusterProfiler and ReactomePA packages against four distinct databases, MSigDB Hallmark, Gene Ontology (GO) Biological Process (BP), KEGG, and Reactome. The most significant pathways were subsequently visualized using dot plots [24, 25].

Rationale and Analysis of Pathway-Specific Module Scores

The expression compendium DGE and ORA results for the total non-responder fibroblast population identified holistic, global gene transcriptional programs that were induced. To dissect this signal and identify which specific fibroblast subtypes are contributing to these enriched pathways, we applied a module score analysis. Bespoke gene sets for each category were derived directly from the list of genes per significant pathway in ORA output. This was to calculate the activity of these ORA-derived pathways at single-cell resolution in a quantitative manner, and make a direct comparison between "Response" and "Non-response" conditions for each of the 9 manually annotated fibroblast subtypes. For the filtered fibroblast object, module scores were computed using AddModuleScore and plotted as faceted violin plots.

Results

Cohort-wide Single-Cell Profiling Identifies 23 Distinct Cell Clusters

We conducted single-cell RNA sequencing on pre-treated pleural effusion samples obtained from seven patients with EGFR-TKI-resistant NSCLC who were subsequently classified into pleural effusion responders (n=3) or non-responders (n=4) to ABCP treatment. Following quality control and filtering, a final number of 16175 high-quality cells were kept for analysis.

Unsupervised clustering of the combined cohort data identified 23 unique cell clusters displayed in UMAP space (Figure 1A). Populations of cells from all seven patients occupied these clusters, demonstrating successful integration and a lack of strong, patient-specific batch effects (Figure 1B). However, when represented based on treatment response (Figure 1C), clear separation between cell types was observed. Some of the largest clusters were also visibly linked, however to a lesser extent, to non response as opposed to response.

Cell Annotation Reveals a Complex Tumor Microenvironment

To formally identify the cellular identities of the 23 clusters, we employed the scType marker-based annotation tool. This analysis successfully assigned a cell type identity to all clusters, confirming the observations from the unsupervised clustering. The TME was revealed

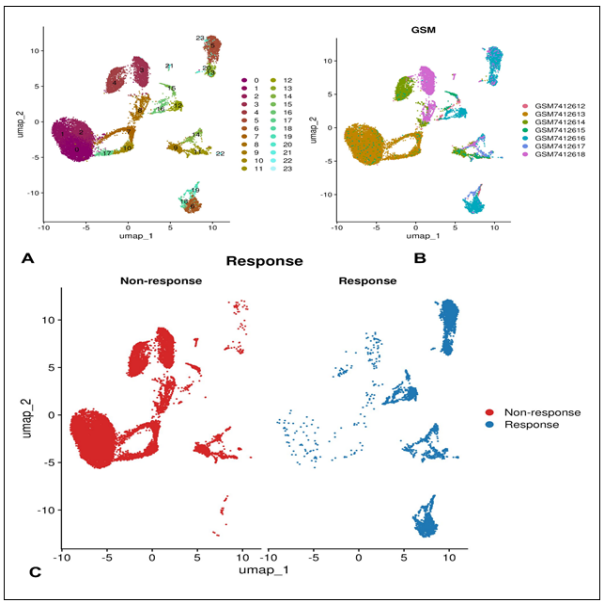

Figure 1. Cohort-wide Single-cell Profiling. (A) UMAP visualization of 16,175 high-quality cells from all patients, colored by 23 distinct unsupervised clusters. (B) UMAP colored by patient sample (GSM ID), demonstrating successful data integration with cells from all seven patients represented across the clusters. (C) UMAP split by therapeutic outcome, visualizing cells from "Non-response" patients (red) and "Response" patients (blue) separately, revealing a distinct separation of cell populations based on clinical outcome.

to be a complex mixture of cell lineages. Major cell types identified included Fibroblasts, Immune system cells, Ciliated cells, Mesothelial cells, and Alveolar macrophages, alongside Pulmonary alveolar type II cells and Ionocytes (Figure 2A). Visualizing these formal annotations on the UMAP, split by response, confirms the stromal-dominant nature of the non-responder TME (Figure 2B).

Compositional Analysis Confirms Stromal Dominance in Non-Responders

To measure the observed changes in TME, we estimated proportions of different cell clusters and cell type profiles looking at samples and conditions. Despite marked patient-to-patient heterogeneity (Figure 2C, 2D), classification of the samples according to therapeutic response revealed distinct compositional changes. Non-responder samples had significantly larger stromal clusters, including above all Fibroblasts, Mesothelial cells and Cilated cells. Responder samples were conversely characterized by an increased relative abundance of immune-related clusters, alveolar macrophages and pulmonary alveolar type II cells.

To confirm the statistical significance of these observations, we considered GLM models for each major cell type based on the corresponding cell counts (Methods 2.4). This analysis confirmed that the pre-treatment TME of non-responders was characterized by a significantly higher proportion of Fibroblasts (FDR < 0.05), Cilated cells, and Mesothelial cells (FDR < 0.05). Conversely, the TME of responders contained a significantly higher proportion of Immune system cells, alveolar macrophages, and pulmonary alveolar type II cells (FDR < 0.05) (Figure 2E). These findings statistically confirm that a pre-treatment TME dominated by stromal components is strongly associated with non-response to ABCP therapy.

Non-Responder TME Displays an Immunosuppressive Cold Signature

Given the significant difference in immune cell infiltration (Figure 2C, 2E), we next sought to characterize the functional state of the immune compartment (Methods 2.5). We calculated module scores for four key immune signatures across all cells annotated as Immune system cells and compared them between response groups. This analysis revealed a complex functional dichotomy. The immune cells in the responder TME displayed a significantly higher CD8+ Cytotoxicity score ($p < 0.001$),

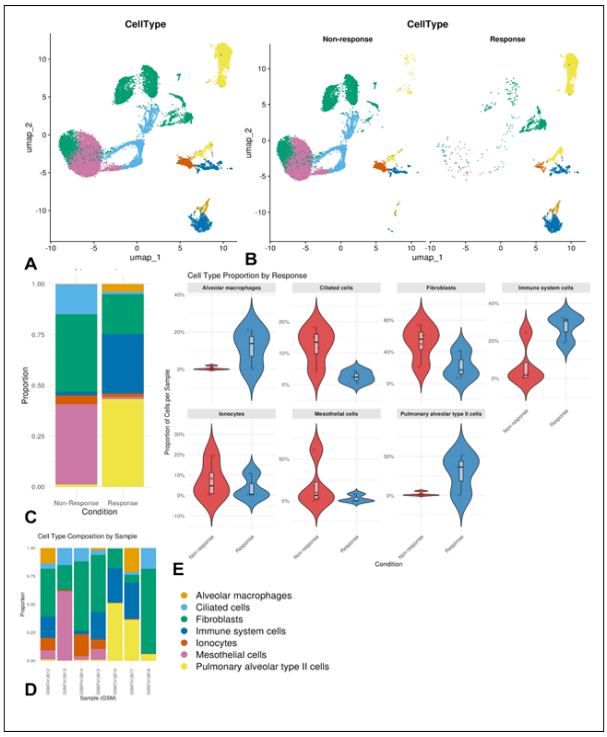

Figure 2. TME Composition Differs between Response Groups. (A) UMAP visualization from Figure 1A, now colored by scType-annotated cell identities, revealing a complex TME. (B) UMAP split by therapeutic response and colored by cell type, illustrating the stromal-dominant (Fibroblast, Mesothelial) TME in non-responders versus the immune-inflamed TME in responders. (C) Stacked bar chart showing the relative proportion of major cell types, aggregated by response condition ("Non-Response" vs. "Response"). (D) Stacked bar chart showing the cell type composition for each of the seven individual patient samples, highlighting patient-to-patient heterogeneity. (E) Violin plots comparing the proportion of major cell types between "Non-response" (red) and "Response" (blue) groups. The analysis confirms a significantly higher proportion of Fibroblasts, Ciliated cells, and Mesothelial cells in non-responders, and a higher proportion of Immune system cells, Alveolar macrophages, and Pulmonary alveolar type II cells in responders (GLM, FDR < 0.05).

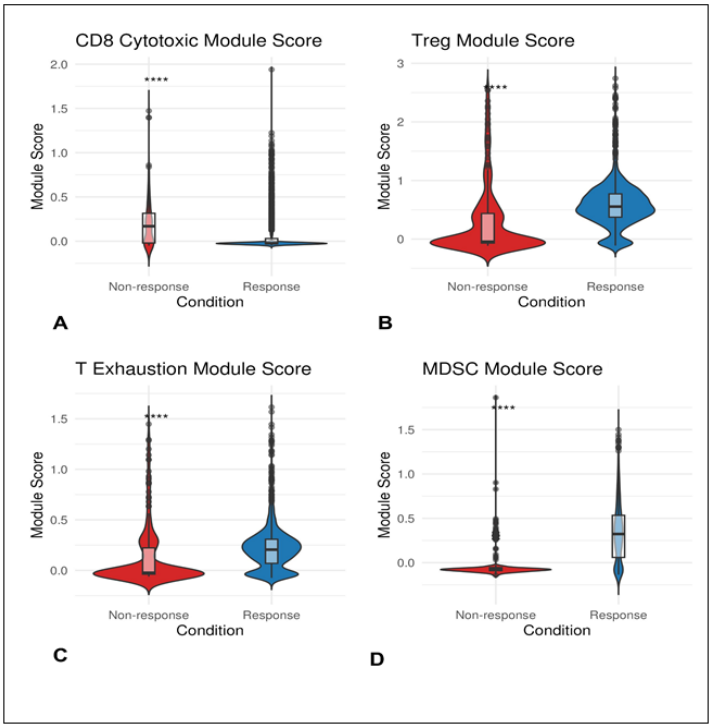

Figure 3. Functional State of the Immune Compartment. Violin plots comparing module scores for key immune signatures within the "Immune system cells" population, split by "Non-response" (red) and "Response" (blue) groups. (A) CD8+ Cytotoxicity score. (B) Regulatory T-cell (Treg) score. (C) T-cell Exhaustion score. (D) MDSC score. Responders show significantly higher scores for all four signatures, indicative of an "inflamed" or "hot" TME that also has co-expressed inhibitory signals. Significance was determined by the Wilcoxon rank-sum test (****$p < 0.001$).

indicative of an active, hot or immune-inflamed microenvironment (Figure 3A). Interestingly, this hot phenotype in responders was accompanied by significantly higher scores for immunosuppressive signatures as well. The responder immune cells also exhibited significantly elevated scores for Regulatory T-cells (Treg) ($p < 0.001$), T-cell Exhaustion ($p < 0.001$), and MDSC ($p < 0.001$) (Figure 3B-D). This suggests that the responder TME may not be purely cytotoxic and rather a highly active, inflamed environment characterized by both potent T-cell activity and the co-expression of inhibitory checkpoint molecules and suppressive cell signatures, a phenotype often predictive of response to checkpoint inhibition.

Fibroblast Sub-clustering Reveals Distinct CAF Compositions Associated with Response

Given that fibroblasts were significantly enriched in the non-responder TME (Figure 2C, 2E), we performed a focused sub-clustering analysis on this population to understand its heterogeneity (Methods 2.6). All cells (n = 5418) initially annotated as Fibroblasts were isolated and re-clustered. Based on the expression of canonical marker genes, these clusters were manually annotated into 9 distinct CAF subtypes: vCAF (vascular CAF), iCAF (inflammatory CAF), GREM1+ CAF, Metabolic-CAF, Hypoxic+ CAF, Prolif F (proliferating fibroblasts), ECM+ CAF, General CAF, and Immunesuppresive IFN-Responsive CAF (Figure 4A).

We next assessed the relative proportions of these 9 CAF subtypes between the response groups. A striking compositional difference emerged. The non-responder TME was overwhelmingly dominated by vCAF, hypoxic-CAFs, metabolic-CAFs, CAFs, ECM+ CAF and GREM1+ CAF subtypes. In sharp contrast, the responder TME showed a different composition, with a notably higher relative abundance of Immunesuppresive IFN-Responsive CAF, iCAF, and Proliferating fibroblasts subtypes (Figure 4B). This compositional skew is also visually evident on the UMAP, where the non-response plot is largely composed of the vCAF and GREM1+ CAF populations (Figure 4C).

Non-Responder CAFs are Transcriptionally Programmed for Matrix Remodeling and Neurogenesis

To understand the functional differences between the fibroblast populations of responder and non-responders, we performed DGE analysis on all fibroblasts, comparing the non-response group to the response group (Methods 2.7). This analysis identified a robust list of 1311 significantly upregulated genes in the non-responder CAFs, including known pro-fibrotic and pro-tumorigenic genes such as POSTN, GREM1, IGFBP5, COL16A1, TGM2, WNT4, FGF9, DKK1, MYL7, NRP2, GAS6, and RGS5.

To identify the biological processes these genes are involved in, we performed ORA using GO, KEGG, and Reactome databases (Methods 2.8). The results consistently pointed to a pro-fibrotic, matrix-remodeling phenotype. Enriched GO terms were dominated by processes such as “actin cytoskeleton organization” (driven by genes like MYL7, ACTG1, ARHGEF12), “cell-matrix adhesion”, and “extracellular matrix organization” (driven by POSTN, CDH11, LAMA3) (Figure 4D). This was

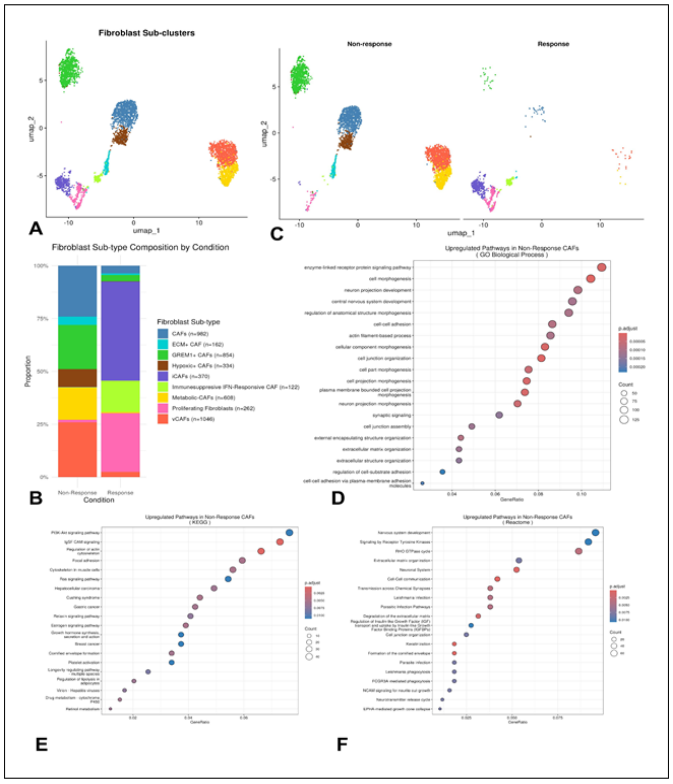

Figure 4. Characterization of the Fibroblast Compartment. (A) UMAP visualization of 5,418 re-clustered fibroblasts, colored by 9 manually annotated Cancer-Associated Fibroblast (CAF) subtypes. (B) Stacked bar chart showing the relative proportion of the 9 CAF subtypes by response condition. Non-responder TMEs are dominated by vCAF, ECM+ CAF, and GREM1+ CAF subtypes, while responder TMEs have a higher abundance of Immunesuppresive IFN-Responsive CAF, iCAF, and Proliferating fibroblasts. (C) UMAP of fibroblast subtypes split by "Non-response" and "Response", visually confirming the compositional skew. (D-F) Over-Representation Analysis (ORA) dot plots of the 1,311 significantly upregulated genes in non-responder CAFs. Enriched pathways are shown for (D) Gene Ontology (GO) Biological Process, (E) KEGG, and (F) Reactome. The analysis highlights pathways for matrix remodeling ("extracellular matrix organization," "actin cytoskeleton organization") and a novel neurogenic-like signature ("nervous system development," "axon guidance"). Dot size represents gene count, and color represents the adjusted p-value.

supported by KEGG and Reactome analyses, which highlighted "Focal adhesion" and key signaling pathways, such as the PI3K-Akt and Ras signaling pathways (driven by EGFR, FGF9, PDGFD, MAPK1) (Figure 4E, 4F). Intriguingly, all three analyses also revealed a strong and unexpected enrichment for pathways associated with "nervous system development", "axon guidance", and "neuron projection", driven by the upregulation of genes such as NRP2, BDNF, DKK1, SEMA5A, and FGFR2. This suggests that the non-responder CAFs may co-opt neurodevelopmental pathways to build the physically-remodeled TME.

Non-Responder Fibroblast Population Shows High Activity for Pro-Fibrotic Pathways

The DGE and ORA analyses identified an aggregate transcriptional program upregulated in the non-response group. To confirm that this program was active across the entire non-responder fibroblast population, we created custom gene modules from the ORA results for four major categories identified above, namely ECM Adhesion, Actin Cytoskeleton, Nervous System, and Signaling Pathways (Methods 2.9).

We calculated module scores for each of these pathways across all fibroblasts. In all four cases, the scores were significantly higher in the non-response group compared to the response group ($p < 0.001$) (Figure 5A-D). This result confirms that the non-responder TME is characterized by a fibroblast population broadly and robustly activating pathways associated with physical matrix remodeling (ECM Adhesion, Actin Cytoskeleton) and pro-tumorigenic signaling (Nervous System, Signaling Pathways).

Key Non-Responder CAF Subtypes Drive the Pro-Fibrotic Transcriptional Program

To deconstruct the aggregate signal observed in the total fibroblast population, we next investigated which specific CAF subtypes were responsible for driving this pro-fibrotic and neurogenic-like program (Methods 2.9). We calculated the module score analysis by our 9 annotated CAF subtypes and compared the scores between response groups within each subtype. This analysis revealed that the pro-fibrotic program was not uniformly active and rather overwhelmingly concentrated within the subtypes associated with the non-responder TME. Specifically, the vCAF, GREM1+ CAF, and ECM+ CAF subtypes all showed robustly high pathway scores in the non-response group (Supplementary Figure 1A-D). This identifies the dominant non-responder populations as the key drivers of this program.

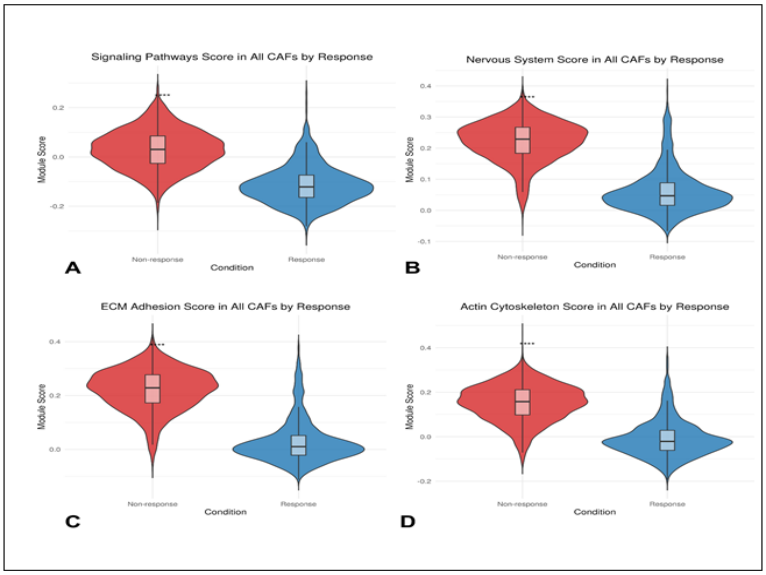

Figure 5. Pro-fibrotic Pathway Activity in All CAFs. Violin plots comparing module scores for four custom gene sets derived from the ORA results in Figure 4. Scores are calculated across all fibroblasts and split by "Non-response" (red) and "Response" (blue) groups. (A) Signaling Pathways score. (B) Nervous System score. (C) ECM Adhesion score. (D) Actin Cytoskeleton score. All four pro-fibrotic and neurogenic-like pathway scores are significantly higher in the total fibroblast population of non-responders. Significance was determined by the Wilcoxon rank-sum test (****$p < 0.001$).

Furthermore, the analysis highlights a critical finding within the iCAF population. Although iCAF cells are more abundant in responders, the iCAF cells that were present in non-responder patients showed significantly and substantially higher scores for all pro-fibrotic pathways compared to the iCAF cells from responder patients. This suggests that iCAF cells can exist in two different functional states, a pro-fibrotic state in non-responders and a different, non-fibrotic state in responders. Conversely, other subtypes, such as the Immunesuppresive IFN-Responsive CAF population prominent in responders, showed uniformly low scores for these pathways in both conditions. This result identifies the dominant non-responder populations (vCAF, GREM1+ CAF, ECM+ CAF), along with a specific pro-fibrotic subset of iCAF cells, as the key drivers of the non-responsive, physically-remodeled TME.

Pro-Fibrotic Gene Signature is Robustly Expressed at the Patient Sample Level

Finally, to ensure these findings were robust at the patient level and not an artifact of cell counts, we analyzed the average expression of the pro-fibrotic pathway genes for each of the 7 patient samples (Methods 2.9). A heatmap of gene expression confirmed a clear separation based on therapeutic response. The four non-responder samples all showed high average expression of the genes associated with ECM Adhesion, Actin Cytoskeleton, Nervous System development, and Signaling Pathways. Conversely, the three responder samples showed uniformly low expression of these same gene sets (Figure 6). This confirms that the pro-fibrotic, neurogenic-like transcriptional program is a stable and defining feature of the entire non-responder TME.

Discussion

In addition to identifying a major pre-treatment divergence in the EGFR-TKI-resistant NSCLC patient TME, the results of this study highlight that this divergence substantially predicts outcome. The NR patients developed a stromal-heavy, non-inflamed, TME

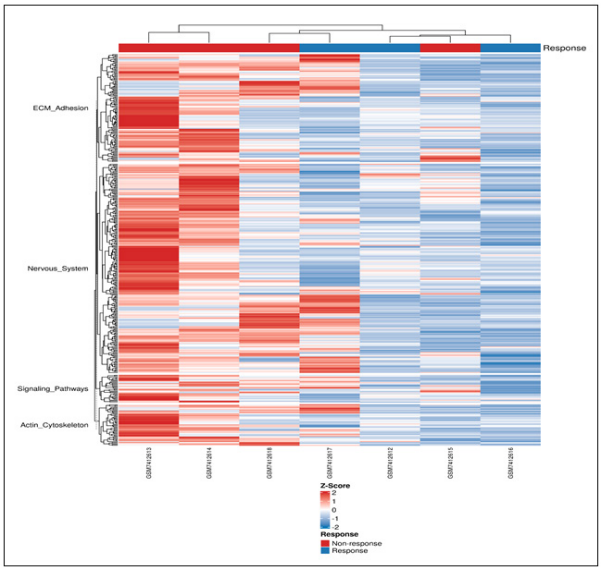

Figure 6. Patient-level Expression of the Pro-fibrotic Neurogenic Signature. Heatmap showing the Z-scored average expression of genes from the four major pro-fibrotic/neurogenic pathway categories (ECM Adhesion, Nervous System, Signaling Pathways, Actin Cytoskeleton). Each column represents one of the seven patient samples, which are clustered by expression similarity. Rows represent the genes within these pathways. The top annotation bar indicates therapeutic response ("Non-response" in red, "Response" in blue), showing a clear and consistent separation of the two patient groups based on this transcriptional signature.

characterized by high numbers of fibroblasts resulting in T-cell excluded environments. In contrast, the R patients exhibited hot, inflamed, TMEs. Unfortunately, the inflamed TMEs of the R group were also exhausted, exhibiting high PDCD1/CTLA4 T-cell exhaustion signatures. Collectively, the hot/exhausted TME creates what may be a biological basis for checkpoint inhibitor clinical efficacy as previously described. The presence of PDCD1/CTLA4 signatures indicates the presence of a specific T-cell population that was successfully primed, trafficked to the tumor and interacted with its tumor specific target, albeit subsequently suppressed. Checkpoint inhibitors are designed to overcome this very suppression. The NR TME, however, lacks the prerequisite T-cell population through which the atezolizumab component can be activated; therefore, there is not a pre-existing immune response associated with the use of atezolizumab and consequently no potential for efficacy.

The NR stromal compartment deconstructed shows an intense, collaborative environment where a defined consortium of CAF subtypes (i.e. vCAF, ECM+ CAF, and GREM1+ CAF) dictate how to sculpt the resistant niche. Each provides a unique contribution toward this construction. ECM+ CAFs, as defined by POSTN, may act as builders of the dense, physical barriers of the extracellular matrix (EMT) preventing T-cell access; vCAFs further contribute by orchestrating aberrant tumor vasculature, thus obstructing immune infiltration and creating an inert hypoxic environment [30]. GREM1+ CAFs act as master regulators by secreting signaling factors that promote fibrogenesis in neighboring cells and may also enhance intrinsic tumor cell aggressiveness, creating a TME that is self-reinforcing for resistance [31]. Transcriptional profiling of these non-responder CAFs corroborated this extreme coordinated architectural activity by demonstrating a large enrichment of pathways suggesting this function (e.g. ECM organization and actin cytoskeletal organization) consistent with previous descriptions of these CAF subtypes [32].

Of note, however, was the identification of a robust neurogenic-like transcriptional program within these NR CAFs, enriched for pathways like axon guidance. This signature, driven by genes including NRP2, BDNF, and DKK1, is proposed to be the functional foundation that CAFs co-opt from neurodevelopmental programs. Normally used by neurons to navigate complex 3D environments and build intricate networks, this molecular machinery is stolen by CAFs to perform an analogous task, to modify the TME, aligning collagen fibers into highways for tumor cell invasion, and erecting a pro-angiogenic, immunosuppressive state [33, 34]. This neurogenic signature provides direct mechanistic explanations for therapy resistance. High NRP2 in vCAFs suggests a pre-existing bypass mechanism for the anti-angiogenic bevacizumab which drug targets VEGF-A, but the NRP2 pathway allows vCAFs to switch to compensatory signaling via VEGF-D, as shown previously for prostate cancer, rendering the bevacizumab component ineffective from the start [35, 36]. The EGFR-TKI resistance that defines this cohort is known to be mediated by DKK1, which imprints fibroblasts into a pro-resistance phenotype, thereby pre-conditioning the TME to fail the next line of therapy [37].

This finding has profound therapeutic implications. Strategies aiming to selectively eliminate bad myCAFs are likely to fail, as the persistent pro-fibrotic signaling environment (driven by factors like TGF-B, DKK1, and BDNF) would simply re-program the remaining good iCAFs to take over the resistance-driving role. This model helps explain the historical failure of many broad stroma-depleting therapies. Even if a drug successfully kills the primary builder CAFs, the architects (the signaling pathways) remain. The surviving iCAFs would simply switch phenotypes and rebuild the resistant stroma. Therefore, the true therapeutic target should not be the CAF subtypes themselves, but the specific, druggable signaling pathways (like the NRP2, BDNF-TrkB, and DKK1 axes) that induce and maintain this plastic, pro-resistance phenotype across the entire stromal compartment.

Rather than definitively driving resistance, this neurogenic signature appears strongly associated with the non-responsive state, suggesting a potential functional role in TME remodeling. The upregulation of genes such as NRP2 and DKK1 suggests that CAFs may co-opt neurodevelopmental pathways to support a T-cell-excluding architecture, though functional validation is required to confirm this causality.

Finally, it is imperative to characterize this investigation as a pilot study, given the restricted cohort size of seven patients (n=3 responders; n=4 non-responders). While the dichotomy observed between immune-inflamed and stromal-neurogenic phenotypes was stark, the small sample size inherently limits statistical power and generalizability. Furthermore, the findings presented here remain purely transcriptomic and correlative. We acknowledge the absence of in vitro or in vivo validation to confirm the hypothesized functional impact of the neurogenic signature on immune exclusion. Consequently, these results should be viewed as a hypothesis-generating framework. Future work is required to not only validate these biomarkers in larger independent cohorts but also mechanistically confirm the CAF-mediated resistance through functional experiments, specifically including CAF–T-cell co-culture systems and targeted knockdown of the identified drivers NRP2, BDNF, and DKK1.

Moreover, the reliance on pleural effusion samples necessitates caution, as this metastatic liquid compartment may not fully recapitulate the spatial architecture and mechanical stiffness characteristic of the primary tumor core. Consequently, the stromal phenotypes observed in this fluidic microenvironment may differ from those in the solid tumor mass, potentially limiting the direct extrapolation of these findings to the primary TME. Future comparative analyses between paired liquid and solid tissue biopsies are essential to distinguish niche-specific adaptations from universal resistance mechanisms. Furthermore, as our current dataset lacks spatial resolution, we cannot definitively confirm the physical exclusion of T-cells or the co-localization of specific CAF

subtypes with immune cells within the tumor architecture. To bridge this gap, future investigations must employ spatial transcriptomics or multiplex immunofluorescence to map the distinct spatial niches of the resistant TME. Such validation is critical to prove that the proposed neurogenic-stromal barrier physically segregates cytotoxic lymphocytes from tumor nests in situ.

The conclusion is repeated with below paragraph please delete the below conclusion and replace this one by:

To summarize the research outlined above, we have established an integrated model for resistance to therapy based on an organism's interaction with its environment. The complex TME is resistant to therapy and can be defined as being made up of elements from multiple tiers of organization within the environment (stroma), which are established through an interaction between all the other spatial, temporal, functional and sequential elements that make up the biological ecosystem (neurodevelopment). These findings are based on data set limitations. The study included a small number of patients and it is important to establish whether the transcriptional data will be predictive biomarkers in future studies with larger sample sizes. Additionally, while pleural effusions are a useful form of metastatic liquid biopsy, they may not accurately represent the primary tumor site within a biosensor, so it is important to validate biomarkers obtained by the sample type collected with respect to each patient accordingly. Now that we have completed an associate analysis of transcriptome data, there is no additional data at the protein level nor is there any data on cellular interactions to confirm the involvement of each of the cellular interactions in the development of the neurogenic signature. Future studies using spatial transcriptomics should be done with this objective in mind to identify the location of T-cell exclusion zones and the CAF subtype that maintained the respective physical resistance niche in order to better understand the activity of CAFs in the development of the neurogenic signature. A robust series of functional studies focusing on NRP2, BDNF and DKK1 are needed to confirm that these markers are true resistance markers. The data presented in this study supports a new class of targets (i.e., neurogenic-stromal) and development of novel stromal-priming strategies using this knowledge for the design and implementation of future clinical trials.

In conclusion, this study proposes an integrated model where resistance is a pre-determined state, identifiable as a complex ecosystem, a stromal-dominant TME built by a collaborative CAF consortium using a co-opted neurodevelopmental function. However, these findings must be interpreted within the context of the study's significant limitations. The patient cohort is small, and the transcriptional signatures must be validated as predictive biomarkers in a larger, independent cohort. The use of pleural effusion samples, while a relevant metastatic liquid biopsy, may not perfectly reflect the primary tumor core. Moreover, the study is transcriptomic and associative, lacking the crucial protein-level validation or spatial context to confirm these cellular interactions. Future directions of the neurogenic signature must be validated as a predictive biomarker. Spatial transcriptomics is required to map the physical resistance niche and confirm T-cell exclusion zones co-localize with these CAF subtypes. Finally, functional studies are needed to prove that these targets (NRP2, BDNF, DKK1) are true drivers of resistance. Despite these limitations, this study provides a strong rationale for stromal-priming strategies, nominating a new class of neurogenic-stromal targets for future trials.

Recommendations and Future Perspectives

Future work should prioritize validating the identified stromal–neurogenic signature in larger, multi-center cohorts and across diverse tissue sources to confirm its predictive utility. Integrating spatial transcriptomics and protein-level imaging will be essential to map CAF–immune cell interactions and verify T-cell exclusion zones. Functional studies targeting NRP2, DKK1, and BDNF-related pathways are recommended to determine whether disrupting these neurogenic-stromal circuits can restore immunotherapy responsiveness. Additionally, developing combination strategies that simultaneously modulate CAF plasticity and enhance T-cell infiltration may offer new therapeutic opportunities. Ultimately, translating these findings into clinically actionable biomarkers could improve patient selection and treatment outcomes.

Strengths of the Research

This research demonstrates several notable strengths, including its use of high-resolution single-cell RNA sequencing to dissect the pre-treatment tumor microenvironment in EGFR-TKI-resistant NSCLC, providing unprecedented cellular and transcriptional insights. The study analyzes real patient-derived pleural effusion samples, increasing clinical relevance, and employs rigorous bioinformatic pipelines for clustering, annotation, and pathway enrichment. By identifying distinct CAF subtypes and uncovering a novel neurogenic-like transcriptional program driving therapy resistance, the work advances mechanistic understanding beyond traditional stromal biology.

Ethical Approval

Not applicable.

Consent to Participate

This study did not involve direct interaction with human participants. Therefore, informed consent to participate was not required.

Consent to Publish

This manuscript does not include any individual person's data in any form (including images, videos, or personal details). All data used are publicly available and anonymized. Accordingly, consent for publication was not necessary.

Competing Interests

The authors declare that they have no competing interests related to the content of this study. No financial, personal, or professional conflicts influenced the design, analysis, or reporting of this work.

Authors contribution

Semaa A. Shaban: Conceptualization, data interpretation, manuscript drafting, and critical revision of the article.Mohammed Abd Hassan: Methodology, data preprocessing, bioinformatic analysis, and validation. Ban Hamid Khalaf: Literature review, results interpretation, and manuscript editing.Ahmed AbdulJabbar Suleiman: Supervision, study design, formal analysis, visualization, and final approval of the manuscript.

All authors reviewed the final manuscript and approved it for submission.

Data Availability Statement

All data supporting the findings of this study are available within the paper and its Supplementary Information

References

1. Bray F, Laversanne M, Sung H, Ferlay J, Siegel RL, Soerjomataram I, Jemal A. Global cancer statistics 2022: GLOBOCAN estimates of incidence and mortality worldwide for 36 cancers in 185 countries. CA: a cancer journal for clinicians. 2024;74(3):229-263. https://doi.org/10.3322/caac.21834
2. Bizuayehu HM, Ahmed KY, Kibret GD, Dadi AF, Belachew SA, Bagade T, Tegegne TK, et al. Global Disparities of Cancer and Its Projected Burden in 2050. JAMA network open. 2024 Nov 04;7(11):e2443198. https://doi.org/10.1001/jamanetworkopen.2024.43198
3. Zamani MR, Šácha P. Immune checkpoint inhibitors in cancer therapy: what lies beyond monoclonal antibodies?. Medical Oncology. 2025 06 19;42(7):273. https://doi.org/10.1007/s12032-025-02822-1
4. Wei J, Li W, Zhang P, Guo F, Liu M. Current trends in sensitizing immune checkpoint inhibitors for cancer treatment. Molecular Cancer. 2024 Dec 26;23(1):279. https://doi.org/10.1186/s12943-024-02179-5
5. Adashek JJ, Moran JA, Le DT, Kurzrock R. Lessons learned from a decade of immune checkpoint inhibition: The good, the bad, and the ugly. Cancer Metastasis Reviews. 2025 04 04;44(2):43. https://doi.org/10.1007/s10555-025-10260-8
6. Naimi A, Mohammed RN, Raji A, Chupradit S, Yumashev AV, Suksatan W, Shalaby MN, et al. Tumor immunotherapies by immune checkpoint inhibitors (ICIs); the pros and cons. Cell communication and signaling: CCS. 2022 04 07;20(1):44. https://doi.org/10.1186/s12964-022-00854-y
7. Zhang Y, Liu Z. Insights into the Mechanisms of Immune-Checkpoint Inhibitors Gained from Spatiotemporal Dynamics of the Tumor Microenvironment. Advanced Science. 2025 09;12(36):e08692. https://doi.org/10.1002/advs.202508692
8. Desbois M, Wang Y. Cancer-associated fibroblasts: Key players in shaping the tumor immune microenvironment. Immunological Reviews. 2021 07;302(1):241-258. https://doi.org/10.1111/imr.12982
9. Ganguly D, Chandra R, Karalis J, Teke M, Aguilera T, Maddipati R, Wachsmann MB, et al. Cancer-Associated Fibroblasts: Versatile Players in the Tumor Microenvironment. Cancers. 2020 09 17;12(9):2652. https://doi.org/10.3390/cancers12092652
10. Jia H, Chen X, Zhang L, Chen M. Cancer associated fibroblasts in cancer development and therapy. Journal of Hematology & Oncology. 2025 03 28;18(1):36. https://doi.org/10.1186/s13045-025-01688-0
11. Yang D, Liu J, Qian H, Zhuang Q. Cancer-associated fibroblasts: from basic science to anticancer therapy. Experimental & Molecular Medicine. 2023 07;55(7):1322-1332. https://doi.org/10.1038/s12276-023-01013-0
12. Wu Z, Luo M, Hu H, Jiang Z, Lu Y, Xiao Z. Hidden forces: the impact of cancer-associated fibroblasts on non-small cell lung cancer development and therapy. Journal of Translational Medicine. 2025 07 25;23(1):830. https://doi.org/10.1186/s12967-025-06791-x
13. Mathieson L, Koppensteiner L, Dorward DA, O'Connor RA, Akram AR. Cancer-associated fibroblasts expressing fibroblast activation protein and podoplanin in non-small cell lung cancer predict poor clinical outcome. British Journal of Cancer. 2024 05;130(11):1758-1769. https://doi.org/10.1038/s41416-024-02671-1
14. Cords L, Engler S, Haberecker M, Rüschoff JH, Moch H, Souza N, Bodenmiller B. Cancer-associated fibroblast phenotypes are associated with patient outcome in non-small cell lung cancer. Cancer Cell. 2024 03 11;42(3):396-412.e5. https://doi.org/10.1016/j.ccell.2023.12.021
15. Sarkar M, Nguyen T, Gundre E, Ogunlusi O, El-Sobky M, Giri B, et al. Cancer-associated fibroblasts: The chief architect in the tumor microenvironment. Front Cell Dev Biol [Internet]. 2023 Jan 30 [cited 2025 Nov 8];11. Available from: https://www.frontiersin.org/journals/cell-and-developmental-biology/articles/10.3389/fcell.2023.1089068/full
16. Masuda H. Cancer-associated fibroblasts in cancer drug resistance and cancer progression: a review. Cell Death Discovery. 2025 07 24;11(1):341. https://doi.org/10.1038/s41420-025-02566-x
17. Zhang H, Yue X, Chen Z, Liu C, Wu W, Zhang N, Liu Z, et al. Define cancer-associated fibroblasts (CAFs) in the tumor microenvironment: new opportunities in cancer immunotherapy and advances in clinical trials. Molecular Cancer. 2023 Oct 02;22(1):159. https://doi.org/10.1186/s12943-023-01860-5
18. Reita D, Pabst L, Pencreach E, Guérin E, Dano L, Rimelen V, Voegeli A, et al. Molecular Mechanism of EGFR-TKI Resistance in EGFR-Mutated Non-Small Cell Lung Cancer: Application to Biological Diagnostic and Monitoring. Cancers. 2021 09 30;13(19):4926. https://doi.org/10.3390/cancers13194926
19. Koulouris A, Tsagkaris C, Corriero AC, Metro G, Mountzios G. Resistance to TKIs in EGFR-Mutated Non-Small Cell Lung Cancer: From Mechanisms to New Therapeutic Strategies. Cancers. 2022 07 08;14(14):3337. https://doi.org/10.3390/cancers14143337
20. Cross D, D'Cruz C, Eberlein C, Spitzler P, Ichihara E, Meador C, Ashton S, et al. 466P - Targeting Resistance in Egfr-Mutant Non-Small Cell Lung Cancer (Nsclc): Preclinical Evidence Supporting the Combination of Egfr Tyrosine Kinase Inhibitors (Tkis) Azd9291 and Gefitinib with Molecularly Targeted Agents and Immunotherapeutics. Annals of Oncology. 2014 09 01;25:iv155. https://doi.org/10.1093/annonc/mdu331.26
21. Tiwari A, Oravecz T, Dillon LA, Italiano A, Audoly L, Fridman WH, Clifton GT. Towards a consensus definition of immune exclusion in cancer. Frontiers in Immunology. 2023;14:1084887. https://doi.org/10.3389/fimmu.2023.1084887
22. Hao Y, Stuart T, Kowalski MH, Choudhary S, Hoffman P, Hartman A, Srivastava A, et al. Dictionary learning for integrative, multimodal and scalable single-cell analysis. Nature Biotechnology. 2024 02;42(2):293-304. https://doi.org/10.1038/s41587-023-01767-y
23. Nader K, Tasci M, Ianevski A, Erickson A, Verschuren EW, Aittokallio T, Miihkinen M. ScType enables fast and

accurate cell type identification from spatial transcriptomics data. Bioinformatics. 2024 07 01;40(7):btae426. https://doi.org/10.1093/bioinformatics/btae426
24. Yu G, He Q. ReactomePA: an R/Bioconductor package for reactome pathway analysis and visualization. Molecular bioSystems. 2016 02;12(2):477-479. https://doi.org/10.1039/c5mb00663e
25. Yu G, Wang L, Han Y, He Q. clusterProfiler: an R package for comparing biological themes among gene clusters. Omics: A Journal of Integrative Biology. 2012 05;16(5):284-287. https://doi.org/10.1089/omi.2011.0118
26. Nair R, Somasundaram V, Kuriakose A, Krishn SR, Raben D, Salazar R, Nair P. Deciphering T-cell exhaustion in the tumor microenvironment: paving the way for innovative solid tumor therapies. Frontiers in Immunology. 2025;16:1548234. https://doi.org/10.3389/fimmu.2025.1548234
27. Mellman I, Chen DS, Powles T, Turley SJ. The cancer-immunity cycle: Indication, genotype, and immunotype. Immunity. 2023 Oct 10;56(10):2188-2205. https://doi.org/10.1016/j.immuni.2023.09.011
28. Guerrouahen BS, Maccalli C, Cugno C, Rutella S, Akporiaye ET. Reverting Immune Suppression to Enhance Cancer Immunotherapy. Frontiers in Oncology. 2019;9:1554. https://doi.org/10.3389/fonc.2019.01554
29. Loriot Y, Sternberg CN, Castellano D, Oosting SF, Dumez H, Huddart R, Vianna K, et al. Safety and efficacy of atezolizumab in patients with autoimmune disease: Subgroup analysis of the SAUL study in locally advanced/metastatic urinary tract carcinoma. European Journal of Cancer. 2020 Oct;138:202-211. https://doi.org/10.1016/j.ejca.2020.07.023
30. Zhang C, Fei Y, Wang H, Hu S, Liu C, Hu R, Du Q. CAFs orchestrates tumor immune microenvironment-A new target in cancer therapy?. Frontiers in Pharmacology. 2023;14:1113378. https://doi.org/10.3389/fphar.2023.1113378
31. Worthley DL, Churchill M, Compton JT, Tailor Y, Rao M, Si Y, Levin D, et al. Gremlin 1 identifies a skeletal stem cell with bone, cartilage, and reticular stromal potential. Cell. 2015 01 15;160(1-2):269-284. https://doi.org/10.1016/j.cell.2014.11.042
32. Belhabib I, Zaghdoudi S, Lac C, Bousquet C, Jean C. Extracellular Matrices and Cancer-Associated Fibroblasts: Targets for Cancer Diagnosis and Therapy?. Cancers. 2021 07 11;13(14):3466. https://doi.org/10.3390/cancers13143466
33. Wei C, Gu Y, Wang W, Ren J, Cui X, Lian X, Liu J, et al. A narrative review of the role of fibroblasts in the growth and development of neurogenic tumors. Annals of Translational Medicine. 2020 Nov;8(21):1462. https://doi.org/10.21037/atm-20-3218
34. Xue M, Zhu Y, Jiang Y, Han L, Shi M, Su R, Wang L, et al. Schwann cells regulate tumor cells and cancer-associated fibroblasts in the pancreatic ductal adenocarcinoma microenvironment. Nature Communications. 2023 07 31;14(1):4600. https://doi.org/10.1038/s41467-023-40314-w
35. Hong S, Yu N, Cho JY, Lee GK, Ahn B, Lee Y, Sim H, et al. VEGF Signal Complexity Confers Resistance to Atezolizumab, Bevacizumab, Carboplatin, and Paclitaxel in EGFR-Tyrosine Kinase Inhibitor-Resistant Non-Small Cell Lung Cancer. MedComm. 2025 09;6(9):e70335. https://doi.org/10.1002/mco2.70335
36. Wang M, Silva CA, Xiong C, Chhoy P, Goel HL, Kumar A, Zhu LJ, et al. Therapeutic blocking of VEGF binding to neuropilin-2 diminishes PD-L1 expression to activate antitumor immunity in prostate cancer. Science Translational Medicine. 2023 05 03;15(694):eade5855. https://doi.org/10.1126/scitranslmed.ade5855
37. Yan R, Fan X, Xiao Z, Liu H, Huang X, Liu J, Zhang S, et al. Inhibition of DCLK1 sensitizes resistant lung adenocarcinomas to EGFR-TKI through suppression of Wnt/β-Catenin activity and cancer stemness. Cancer Letters. 2022 04 10;531:83-97. https://doi.org/10.1016/j.canlet.2022.01.030